Geoderma 430 (2023) 116348

Contents lists available at ScienceDirect

Geoderma

journal homepage: www.elsevier.com/locate/geoderma

Observations of intra-peatland variability using multiple spatially coincident remotely sensed data sources and machine learning

Dave O'Leary [a], Colin Brown [a], Mark G. Healy [b], Shane Regan [c], Eve Daly [a,*]

[a] Hy-Res Research Group, Earth and Ocean Sciences and Ryan Institute, College of Science and Engineering, University of Galway, Galway H91 TK33, Ireland
[b] Civil Engineering and Ryan Institute, College of Science and Engineering, University of Galway, Galway H91 TK33, Ireland
[c] Science and Biodiversity Unit, National Parks and Wildlife Service, Dublin, Ireland

ARTICLE INFO

Handling Editor: Budiman Minasny

Keywords:
Self-organising maps
Unsupervised classification
Peatland restoration
Optical satellite data
Airborne geophysics

ABSTRACT

Peatlands are important sites of ecosystem services, particularly as soil carbon stores, and are recognised in many international climate strategies. However, drained peatlands, which have been modified for industrial extraction or agriculture, are responsible for carbon emission. Peatland restoration aims to return these degraded sites to a natural state. Multiple means of remotely monitoring the success of peat restoration are available, ranging from space-based satellite measurements (optical and radar) to airborne geophysical measurements (electro-magnetic and radiometric). This paper integrates multi-band, spatially coincident, remotely sensed data into a single framework, resulting in a comprehensive interpretation of intra-peatland variation of key restoration indicators. It uses a semi-automatic, data driven approach with unsupervised neural network machine learning clustering. A Multi-Cluster Average Standard Deviation metric is introduced which can determine the appropriate number of clusters for any dataset. The method was applied to a site in Ireland, representative of degraded peatlands, where optical satellite and airborne radiometric geophysical measurements were combined. The method was successful at determining the appropriate number of clusters for single and combined datasets, and the resulting cluster signatures provided visually compelling representations of the intra-peatland variation. This resulted in a comprehensive interpretation of intra-peatland variation of several key peatland restoration indicators, namely surface vegetation levels and soil moisture to ~ 60 cm of the peat surface. The study provides a framework for high spatial and temporal resolution monitoring of peatland restoration using future drone-based platforms.

1. Introduction

Peatlands are recognised as significant ecosystems for biodiversity, water system services and carbon (C) stores (UNEP, 2022). The United Nations Framework Convention on Climate Change (UNFCCC) highlighted peatlands as a priority via the introduction of the Wetlands Drainage and Rewetting (WDR) activity under Article 3.4 of the Kyoto Protocol (UNFCCC, 2011). Peatlands account for 5 – 30 % of soil C stock (Minasny et al., 2019; UNEP, 2022) while covering only ~ 3 % of the earths land surface (Xu et al., 2018). Drained/degraded peatlands, used for industrial extraction, forestry, or agriculture (pasture), are responsible for emissions which are affecting the global C balance (Evans et al., 2021; Qiu et al., 2020; UNEP, 2022).

The goal of peatland restoration is to return modified peatlands to their natural state, usually via changes to water table depth and vegetation (Monteverde et al., 2022), with water table management being a key environmental control on C exchange between the soil and atmosphere (Wilson et al., 2022). Peatlands which have been historically drained and undergone restoration appear to be non-uniform in recovery, creating "locally novel ecosystems" (Kreyling et al., 2021). Spatial changes in depth to the water table will have consequences for several ecosystem functions such as plant community composition, water runoff and nutrient cycling (Kasischke et al., 2009). This implies that restoration plans require local measurement of properties within a peatland before and after restoration in order to measure success (Heger et al., 2022; Renou-Wilson et al., 2019). The two main requirements to determine the effectiveness of a peatland restoration are ecological and hydrological monitoring (Mackin et al., 2017). Ecological monitoring represents mapping spatially and ecologically distinct features for the measurement of landscape structure and change. Hydrological monitoring is focused on environmental factors such as water table depth, flow, and hydrochemistry. Both require monitoring prior to, during and

* Corresponding author.
E-mail address: eve.daly@universityofgalway.ie (E. Daly).

https://doi.org/10.1016/j.geoderma.2023.116348
Received 4 November 2022; Received in revised form 17 January 2023; Accepted 17 January 2023
Available online 24 January 2023

after restoration into the future.

There are several established and emerging remote sensing techniques that can be used to measure peatland properties (Minasny et al., 2019) and they have advantages over more traditional methods (e.g., large areas, consistent spatial sampling). These can include satellite remote sensing (Bhatnagar et al., 2020), airborne geophysical surveys (Boaga et al., 2020), drone-based surveys (Dronova et al., 2021), and ground geophysics (Altdorff et al., 2016). Optical satellite and airborne radiometric data are analysed in this paper.

Satellite remote sensing methods (optical and radar) are prominent in the peatland mapping literature (Czapiewski and Szumińska, 2022). For example, the Sentinel program (Sentinel, 2022) is a series of earth observation missions performed by the European Space Agency and European Commission initiative, Copernicus. This program provides free access to optical (Sentinel-2) and radar (Sentinel-1) data at spatial resolution of ~ 10–30 m and a temporal resolution of between 3 and 10 days, depending on the satellite mission. These have become popular as they provide consistent spatial and temporal resolution and are sensitive to physical properties related to peatland identification and monitoring (Minasny et al., 2019) as they are sensitive to landcover (optical) and the near surface (radar) to a depth of ~ 10 cm.

Optical sensors on satellites record multiple bands of electromagnetic energy as reflectance values, ranging from the visible to shortwave infra-red. These values can be used to identify landcover type via "spectral signatures" and seasonal changes in landcover via changes to these signatures (Aune-Lundberg and Strand, 2021; CORINE, 2018). However, optical data are degraded or non-existent in the presence of cloud cover/shadow, which reduces the temporal resolution in temperate regions (Connolly, 2019). Often, indices (mathematical combinations of data bands that produce a single number which is sensitive to particular physical properties of interest) are used (Czapiewski and Szumińska, 2022; Wang and Qu, 2009). Of these, Normalised Difference Vegetation Index (NDVI), Enhanced Vegetation Index (EVI) and Normalised Difference Water Index (NDWI) are popular (Frampton et al., 2013). Within a peatland these and other indices can yield information on landcover types such as bare peat and vegetation (Bhatnagar et al., 2020) at a resolution of ~ 10 – 30 m.

Airborne geophysical surveys are suited to peatland mapping (Airo et al., 2014; Berglund and Berglund, 2010; Boaga et al., 2020), as they cover large areas quickly and consistently (Ameglio, 2018; Binley et al., 2015) and are sensitive to subsurface physical properties such as density, porosity, and water content. National airborne geophysical surveys which include electromagnetic and gamma-ray spectrometry (radiometric) data can be used in regional and local scale peatland studies (Beamish and Young, 2009; Berglund and Berglund, 2010; Siemon et al., 2020).

Airborne radiometric surveys measures the naturally occurring radiation emitted by radionuclides in geological material (Minty, 1997). Typical elements of interest are Potassium (^{40}K), Uranium (^{238}U) and Thorium (^{232}Th) (Reinhardt and Herrmann, 2019). These are recorded as energy bands in counts per second (cps), with a 4th Total Count (TC) measurement recorded for the full energy spectrum. While it has historical applications in the mineral industry (Shives et al., 2000) and geological mapping (Martelet et al., 2006), recent studies have begun to recognise the potential of radiometric data in soil (Beamish, 2015; Marchant, 2021; Priori et al., 2014) and, in particular, peat mapping (Beamish, 2014; O'Leary et al., 2022; Siemon et al., 2020).

As peat is a non-radioactive material, several studies have attempted to link radiometric data to peat thickness estimation (Gatis et al., 2019; Keaney et al., 2013; Siemon et al., 2020). However, attenuation models (Beamish, 2013) show that 90 % of radiometric signal is attenuated in ~ 60 cm of typical peat, therefore limiting peat thickness estimation but may have potential for mapping peatland extent (O'Leary et al., 2022) and subsurface physical properties within this depth range. Soil moisture variation in this layer may be responsible for radiometric signal variation as water is a strong attenuator (Beamish, 2013; Endrestøl, 1980). It is likely that a complex combination of thickness and soil moisture are the biggest drivers of radiometric signal variation within a peatland (Reinhardt and Herrmann, 2019); however, vegetation may also have an attenuation effect (Minasny et al., 2019; Minty, 1997).

Peatlands are complex ecological and hydrological environments (Price et al., 2003). The influence of such complexity within a peatland requires simultaneous analysis of multiple data sources over a site in order to extract meaningful and comprehensive information about peatland processes (Kreyling et al., 2021; Räsänen et al., 2022). Machine learning, which is becoming prevalent in geoscience (Dramsch, 2020), has the ability to exploit non-linear statistical relationships between data bands to aid in data visualisation and model building. Unsupervised machine learning can achieve this, using the concept of exploratory data analysis (EDA; (Chatfield, 1986). EDA aims to (1) maximise insight into a data source, (2) visualise potential relationships between data vectors, (3) detect data vectors that vary significantly from others, (4) develop an explanatory model of the data source, and (5) extract relevant data bands from the overall data source.

Clustering (synonymous with the term classification) is the grouping together of multi-band data vectors (Kaufman, 2005), where the grouped input data vectors are statistically similar to each other. Many clustering techniques have been developed such as centroid, hierarchical, density and spectral clustering, each with their own advantages and disadvantages (Benabdellah et al., 2019; Delgado et al., 2017). See Table 1 for a list of descriptors used in this paper.

The aim of this paper is to develop a data driven, objective, and semi-automatic technique to determine the range of appropriate number of clusters, using an unsupervised classification of spatially coincident data bands from multiple data sources. This has implications across many domains of research. The technique is demonstrated in this paper using 4 bands of airborne radiometric and 13 bands of optical satellite data over previously delineated peatlands (O'Leary et al., 2022). These datasets, which ideally should be spatially and temporally coincident, are related to spatial physical property variation (landcover and soil moisture), which are important indicators of restoration success (Mackin et al., 2017). The methods presented provide a framework to perform an initial investigation prior to a peatland restoration program and a means to monitor success of such a program into the future (Mackin et al., 2017). They have implications for integrated interpretations of datasets from multiple sensors, including those in future high-resolution drone-based applications.

2. Materials and methods

2.1. Clustering

2.1.1. Self-Organising Maps

Traditional centroid-based clustering methods, such as K-Means (Gersho, 1982), rely on minimising the distance between data vectors and a finite number of cluster signatures in the dataspace. Self-

Table 1
Definitions of data descriptors in text.

Name:	Definition:
Data Source	A single source of spatially and temporally coincident data (e.g., Sentinel-2 data from a single date, radiometric data)
Data Band	A single stream of data from within a data source (e.g., Sentinel-2, Band 8 or radiometric, K cps)
Data Vector	All data that are located on a single spatial coordinate from described data bands and data sources (e.g., Sentinel-2, 13 bands become a data vector of 13 numbers at spatial location x, y)
Data Space	The virtual multi-dimensional space with as many axes as there are data bands being analysed
Cluster	A single identifier for a subset of input data vectors (e.g., Cluster 1 contains x number of input data vectors)
Cluster Signature	A single data vector that can describe all data vectors associated with a particular cluster

Organising Maps (Kohonen, 2013) rely on competitive learning within a neural network to assign any data vector to a particular cluster (Valentine and Kalnins, 2016). This is a form of unsupervised classification (Kiang, 2001) and is considered suitable where the goal is to visualise multi-dimensional data (Benabdellah et al., 2019) by exploiting non-linear statistical relationships between datasets that traditional (linear) methods (correlation, regression, etc.) cannot capture.

In order to cluster the data within the Self-Organising Maps algorithm (Kohonen, 2013), a number of cluster signatures must be "initialised". These contain the same number of bands as the data vectors and are initially assigned random values in the data space. A data vector is compared to each cluster signature, via a data space distance metric, and the "winning" cluster is assigned. The winning cluster signature is updated to be more numerically similar to the data vector it represents. This process takes place for all input data vectors iteratively until each is assigned to a cluster. Each cluster signature is then said to represent a set of input data vectors that are numerically similar to it. See Appendix A supplementary material.

Determining the appropriate number of clusters for a dataset is difficult (Benabdellah et al., 2019; Delgado et al., 2017) often requiring subjective, a priori, or expert knowledge of the clustering algorithm. Clusters are chosen based on an expected or known number (Marsh and Brown, 2009). Frequently, clustering validation tools are used (Benabdellah et al., 2019) to determine if the number of clusters is statistically significant. These calculate several internal statistics such as the Calinsku-Harabasz index (Caliński and Harabasz, 1974), Connectivity index (Xing et al., 2005), or the Davies-Bouldin index (Davies and Bouldin, 1979).

2.1.2. Appropriate number of clusters

The simple and novel approach presented here expects that the appropriate number of clusters for a set of input data vectors is any which returns similar cluster signatures after multiple clustering attempts. To achieve this, the clustering process is performed multiple times (e.g., 100 loops) for an increasing number of clusters, starting with 1 and increasing to X (e.g., 20) cluster signatures (Fig. 1). For each clustering loop the distance, in the data space, between the cluster signature and each associated data vector is calculated and saved. Then, the standard deviation of distance is calculated for each data vector once all loops are complete. Finally, an average of the standard deviations is calculated, resulting in the Multi-Cluster Average Standard Deviation (MCASD) metric. The aim of a MCASD analysis is to facilitate the choice of highest number of clusters, and therefore the highest spatial resolution, without compromising the stability of the solution, which is determined from multiple clustering loops. A low value of MCASD is a consequence of repeatable cluster signatures, despite random initialisation (Delgado et al., 2017), and is an indication that the associated number of clusters is appropriate to describe the range of input data vectors. A maximum of 100 loops and 20 clusters proved adequate to determine which number of clusters is appropriate for the data in this study.

2.1.3. MCASD in practice

To demonstrate the MCASD method on spatial data, a data source with a known number of clusters was used as input data vectors. This synthetic data source has previously been used in an example of the application of Self-Organising Maps to geospatial data (Marsh and Brown, 2009). It can be considered analogous to a geo-spatial dataset as it shows a varying background with a non-distinct border and anomalous structures, where each pixel has an assigned geographic coordinate. A graph of the MCASD metric against number of cluster signatures (Fig. 2-A) shows that 1 – 4 clusters are appropriate to visualise this data source.

The data source is a greyscale image of rice grains which are randomly orientated within a variable background intensity (Fig. 2-B). The image consists of 65,536 data vectors organised as a single data band with a brightness value ranging between 1 and 256. This image can be broken into four groups, (1) bright background, (2) dark background, (3) rice on light background, and (4) rice on dark background. Fig. 2-C shows the output of the first cluster loop when the number of clusters is 4 and shows the expected classifications with some minor misclassification present. See Appendix A supplementary material for further descriptive diagrams and animations.

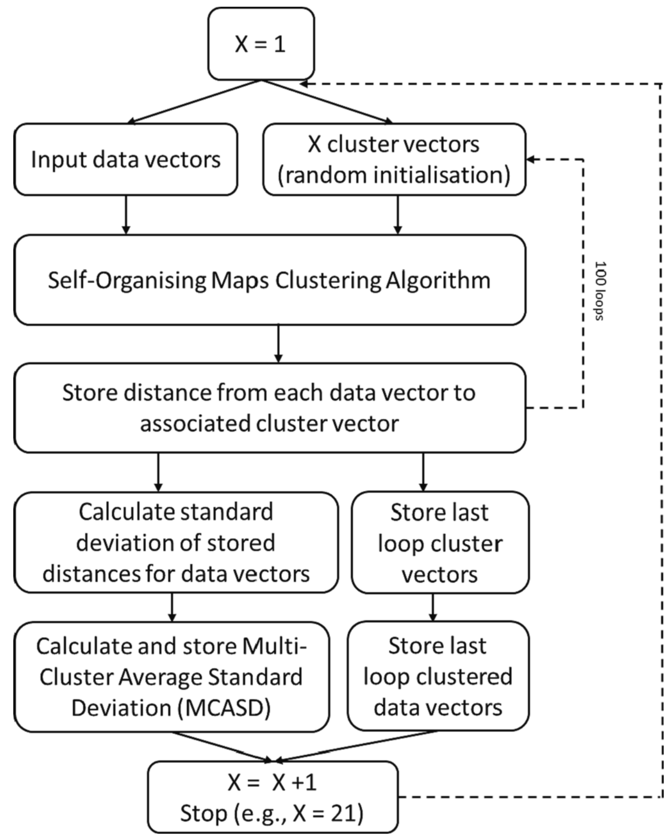

Fig. 1. Multi-Cluster Standard Deviation (MCASD) flowchart.

This clustering method does not take coordinates of the pixel into account, but instead groups data based on similarity between the various data layers (in this case a brightness value). Each data vector is then given a number (1 – 4 for example) representing which cluster it belongs to. The data vectors are then reprojected back to their respective location in the image and coloured based on this number. The resulting spatial distribution is related to geographical locations where data are similar.

The spatial distribution would change with the number of clusters used, however the purpose of MCASD analysis is to provide confidence that the number of clusters chosen, and that the spatial distribution of the clusters is relevant and appropriate.

2.2. Site

A site in central Ireland was chosen because (1) it is typical of those industrial peatlands in the northern hemisphere being targeted for restoration (Bord na Móna, 2021), (2) there are ground-based datasets to constrain the interpretations in this paper, and (3) spatially coincident Sentinel-2 (S2) and radiometric datasets are available.

Garryduff peatland (Lat: 53.25° N, Long: 8.08° W) is a former raised bog, and has been an extraction site from 1968 until 2019 (Bord na Móna, 2021) (Fig. 3-A). The site is described as ~ 50 % bare peat, with active drainage channels, standing water and emerging wetland vegetation making up the rest. Peat thickness on site is generally greater than ~ 50 cm (Bord na Móna, 2021). The site was actively pumped to

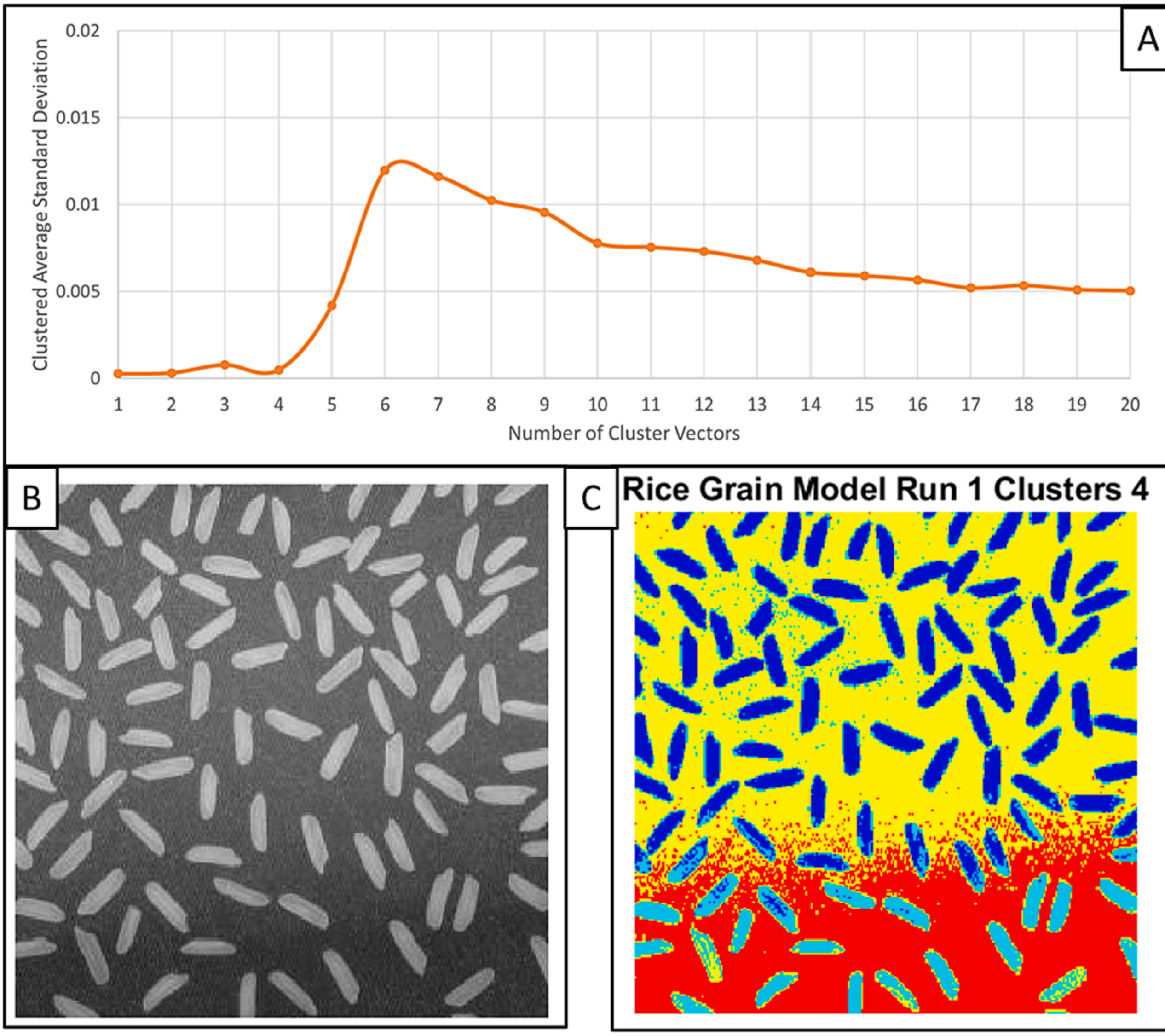

Fig. 2. A) MCASD graph for maximum of 20 experimental cluster signatures. B) Original Grey scale image C) Clustered output coloured by cluster number.

maintain an artificially deep water table.

The peatland boundaries (Fig. 3-B) were defined using radiometric data (O'Leary et al., 2022) and a supervised machine learning methodology. This resulted in a 50 × 50 m resolution raster, delineating pixels which have been defined as either Peat or non-Peat. O'Leary et al. (2022) demonstrate that the technique improves delineation of peat boundary and peat under modified landcover compared to recognised national databases (CORINE, 2018). Therefore, only the 16,633 pixels (~4,200 ha) that fall within areas defined as peat (Fig. 3-B) are carried forward for further analysis.

The underlying bedrock is recorded to be limestone and shale (GSI, 2022a) and the quaternary sediment is a mixture of "cut over raised peats", "alluvium" (close to the rivers) and "till derived from limestone" (GSI, 2022b). Landcover classification (Fig. 3-C) from the European Space Agency (CORINE, 2018) shows a mixture of peat bog, grassland and forestry but provides no information on soil type. The CORINE 2018 landcover map has a resolution of 25 ha (CORINE, 2018), and has been converted to a raster with 50 × 50 m resolution for visualisations within this study.

2.3. Optical satellite data

S2 satellites were only launched in June 2015 and no cloud-free images from the study site were acquired during June 2016, when the radiometric data source was acquired, highlighting the issue of cloud cover inherent in the use of all optical satellite data in temperate latitudes such as Ireland (Connolly, 2019). As an alternative to a temporally coincident dataset, two Level 1-C S2 images, acquired on 20/06/2017 and 28/06/2018, were downloaded from the Copernicus Hub (https://scihub.copernicus.eu). These dates were chosen as they were (1) cloud-free over the study site and (2) were acquired at a similar time of the year as the radiometric data source in this study (see section 2.4). The temporally and seasonally closest cloud-free S2 image was acquired in June 2017. In order to verify that this image is representative of the landcover variation at the time of radiometric data acquisition, a second image, acquired in June 2018 was also analysed to establish that landcover did not significantly change from one year to the next.

DOS1 atmospheric correction (Chavez, 1996) was applied to all S2 data bands in QGISv3.16 using the SCPv7.10.5 plugin (Congedo, 2021). The data were re-projected to a common reference system (EPSG: 2157 – Irish Transverse Mercator) and resampled to 50 × 50 m resolution, required to match "pixel to pixel" to other datasets used in this study.

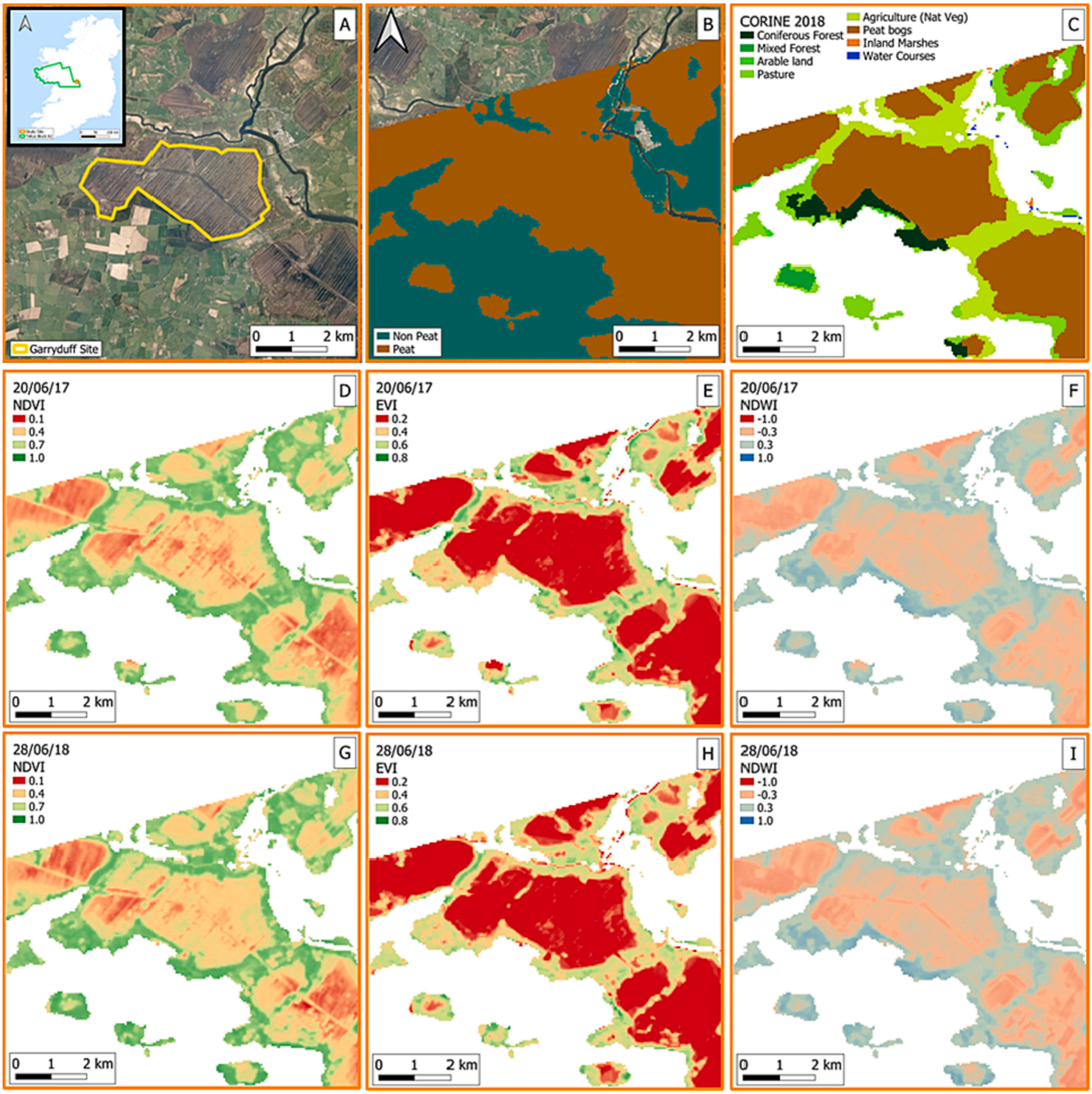

Fig. 3. A) Aerial image with industrial peatland boundary with inset showing Tellus Radiometric Block A2 and study location within Ireland. B) Peat vs non Peat extent for the study site edited from O'Leary et al. (2022) (Fig. 6) highlighting the spatial extent of data used in this study. C) CORINE 2018 landcover classification. D) - I) S2 images of NDVI, EVI, and NDWI for days in summer 2017 and 2018. North Arrow in B is relevant for all images.

The standard indices (Bhatnagar et al., 2020), highlighted in Section 1, were calculated to visualise and compare the two S2 data sources (Fig. 3-D to 3-I).

2.4. Airborne geophysical data

The Tellus survey (GSI, 2022c) is a national airborne geophysical acquisition survey that acquires spatially consistent data covering Ireland. It collects three coincident geophysical datasets, electromagnetic, magnetic, and radiometric. The data are acquired in acquisition blocks with similar acquisition parameters. Survey lines are flown at 345° and a line spacing of 200 m and ground clearance of 60 m. However, this is occasionally exceeded due to terrain or flight restrictions.

Radiometric data were collected at 1 Hz, which equates to ~ 60 m sample spacing along flight lines. Data processing is performed by the contractor and follows international guidelines (IAEA, 2003). The radiometric data in this study were selected from the Tellus Block A2 (Fig. 3-A). A total of 6,445 datapoints were acquired over the Garryduff site as a set of 25 flight lines (~387 line km's) on 3rd June 2016. The data bands were downloaded as elemental concentrations for Potassium (K), Uranium (U) and Thorium (Th) and converted to counts per second (cps) via sensitivity values, which are contractor provided values to convert recorded gamma ray counts per second to an elemental concentration (SGL, 2017). The Total Count (TC) data band is provided in cps. Each data band was then interpolated using minimum curvature to a 50 × 50 m grid and QGISv3.16 was used for visualisation and GIS analysis (Fig. 4-A to 4-D). All data were reprojected to the common reference system. The interpolation, along with the inherent low signal environment that peatlands present (Beamish, 2014), are the cause of negative values in the radiometric signal. While not physically possible, they are not removed from this analysis as the neural network methods rely on statistical relationships between the data bands, not their absolute values.

2.5. Data organisation and traditional analysis

S2 images (13 optical bands), and the radiometric (4 cps bands) data sources were analysed separately using the MCASD method. Each S2 image was also combined with the radiometric data source and analysed as an integrated, 17 band, data source. Data bands were placed into columns and normalised (with each column scaled between 0 and 1), to remove scaling bias between bands. Once MCASD analysis was complete, the results were presented as a MCASD graph, similar to Fig. 2-A, a raster map showing the spatial distribution of the clusters and a unique cluster signature graph, similar to a "spectral signature graph" (Huete, 2004) used in S2 classification applications.

Linear correlation analysis was performed between S2 indices (Fig. 3-D to 3-I) and radiometric data bands (Fig. 4-A to 4-D) to justify the selection of S2 data source and the use of non-linear machine learning over traditional data analytical methods. This analysis was also performed between four radiometric data bands and peat thickness data (Bord na Móna, 2021) (See Appendix A supplementary material for diagram) from within the Garryduff site boundary (Fig. 3-A) to aid discussion on intra-peatland variation of radiometric signal.

One possible means to identify intra-peatland variation of radiometric signal is through the use of Horizontal Gradient Magnitude (HGM) analysis (Beamish, 2016), which highlights areas of changing radiometric signal. This analysis was applied to the TC band of the radiometric data source (Fig. 6-D) as a comparison to the machine learning method presented here.

3. Results

3.1. Linear correlation analysis

Correlation was performed between four radiometric data bands and a peat thickness data source (Bord na Móna, 2021), where there were 3,554 coincident data vectors. This returned correlation coefficients of: K cps: −0.04, U cps: 0.19, Th cps: −0.06 and TC cps: 0.25. These correlation results indicated a weak link between radiometric band variability and peat thickness variability within the Garryduff site boundary (See Appendix A).

Correlation was also performed between the four radiometric data bands and the S2 indices (Fig. 3-D to 3-I). These results indicated a moderate correlation between the radiometric data bands and the relevant indices, with the correlation being marginally higher for 2017 S2 data source (Table 2).

3.2. MCASD on S2 data sources

The top row (Fig. 5) from MCASD analysis shows that four clusters are appropriate when clustering S2 data from 20/06/17 and that three clusters are appropriate for S2 data from 28/06/18. The middle row

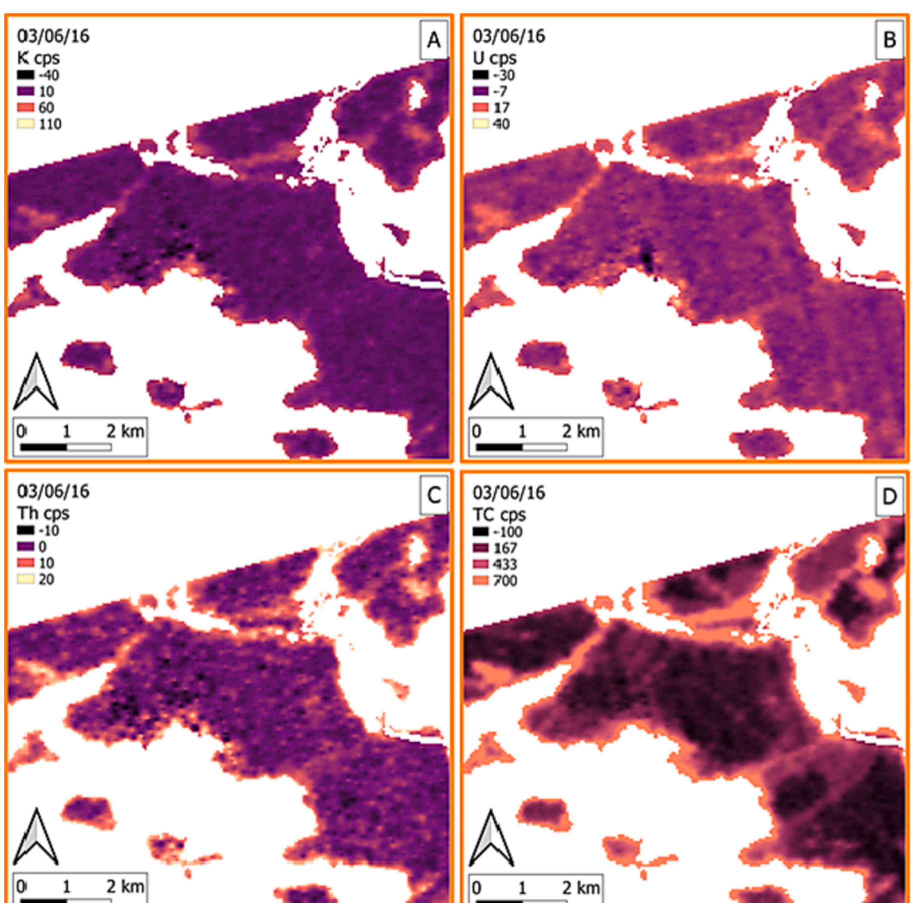

Fig. 4. A) Tellus Radiometric K cps. B) Tellus Radiometric U cps. C) Tellus Radiometric Th cps. D) Tellus Radiometric TC counts per second (cps).

Table 2
Correlation coefficients between radiometric data bands and calculated S2 indices.

	NDVI 2017	EVI 2017	NDWI 2017	NDVI 2018	EVI 2018	NDWI 2018
K cps	0.53	0.57	0.54	0.51	0.57	0.52
U cps	0.46	0.50	0.45	0.43	0.49	0.43
Th cps	0.53	0.56	0.52	0.50	0.56	0.51
TC cps	0.71	0.75	0.71	0.68	0.74	0.89

shows the unique signature (Huete, 2004) for each cluster signature. Both data sources had similar cluster signatures in terms of amplitude of band values. The bottom row shows the spatial distribution for the associated clustered result for each S2 data source. The main difference between the MCASD results is that the rededge1 (B5) amplitude is significantly larger in S2 data from 2018, compared to 2017. From the spatial distribution and cluster signature plots, it appears that Cluster 3 (2018) is comparable to Clusters 3 and 4 (2017).

3.3. MCASD on radiometric data

The MCASD graph (Fig. 6-A) shows that 2 – 5 clusters may be used to group these radiometric data bands. The 5-cluster result is then shown via the unique cluster signature plot (Fig. 6-B) and the spatial distribution map (Fig. 6-C).

The cluster signature plot of normalised radiometric values shows that radiometric signal is relatively high for all four bands in Cluster 1 and low in Cluster 5. The spatial distribution of these clusters shows that Cluster 1 is generally found around the edges and Cluster 5 is located in the interior of the peatland areas.

There is potential for spatial variability in the sub-peat radiometric source intensity to be a factor in intra-peatland signal variation (Beamish, 2014). However, the study site is underlain by a single geological unity (GSI, 2022a) and so it is assumed that the sub-peat source of gamma rays is spatially constant.

Horizontal Gradient Magnitude analysis was applied to the TC band of radiometric data source (Fig. 6-D). Areas of high values (red) indicate a changing radiometric signal in this band and areas of low values (blue) indicate areas of stable signal (Beamish, 2016). The edges of the peatland show the highest value, as the data pass from non-peat to peat soils (O'Leary et al., 2022) and intra-peatland variation of radiometric signal is also highlighted.

3.4. MCASD on combined S2 and radiometric data

S2 data bands were combined with radiometric data bands to provide a single integrated data source originating from the landcover and the subsurface to a maximum depth of ~ 60 cm. The 2017 S2 data bands, combined with radiometric data bands, are shown (Fig. 7). The results, when combined with 2018 S2 data bands, are very similar (See Appendix A supplementary material for diagrams).

The MCASD analysis determines that three clusters can be used to appropriately group these data bands (Fig. 7-A). The spatial distribution of these clusters (Fig. 7-B) shows that Cluster 1 is generally located at the edges and Cluster 3 is generally located towards the centre of defined peatlands.

The cluster signatures (Fig. 7-C) for S2 bands are shown in absolute values and radiometric bands are shown in normalised values as the absolute dynamic ranges of S2 and radiometric data sources are significantly different. Cluster 1 shows elevated values of S2 green (B3) and S2 red edge to near infra-red (B5 - B8A) and high radiometric band values. Cluster 2 has mid-range values of both B5 - B8A and radiometric bands. Cluster 3 is defined by low B5 - B8A bands, high S2 short wave infra-red (B11 – B12) and low radiometric band values.

4. Discussion

4.1. Intra-peatland landcover mapping from S2 data

The S2 optical satellite data provided a means to analyse the intra-peatland landcover variation as a function of time, a proxy ecological indicator for vegetation (Bhatnagar et al., 2020). All 13 bands of the S2 data source were included in the analysis. The majority of the literature uses limited data bands to calculate indices, representative of the landcover type of interest (Arekhi et al., 2019; Hird et al., 2017; Maduako et al., 2017). Bhatnagar et al. (2020) used a combination of 10 bands alongside several indices in a machine learning prediction framework. However, to the authors' knowledge, no studies have yet combined the aims of exploratory data analysis (Chatfield, 1986) and unsupervised neural network clustering with full spectrum S2 data.

Indices have been traditionally derived due to physical relationships between relevant data bands and landcover of interest (Gao et al., 2000; Liu and Huete, 1995) and tend to be universally applicable and not necessarily site specific (Frampton et al., 2013). By including all 13 S2 data bands in this analysis, the results were not biased by any subjective choice of indices and were focused on the site under investigation. The standard indices calculated here showed the S2 data from 2017 and 2018 to be similar (Fig. 3-D to 3-I); however, none of them included B5, the red edge component, which showed significant discriminatory power (Fig. 8) that might otherwise have been missed.

The choice of the appropriate number of clusters has been determined by MCASD analysis. The spike noted when MCASD was performed for three clusters in the 2017 S2 data source (Fig. 5-A) indicated that three was not an appropriate number of clusters for this data source. The MCASD analysis prevents the use of the three-cluster result in any further analysis. See Appendix A for explanatory diagram.

The spatial distribution of both S2 MCASD analysis are shown with visual comparison from CORINE 2018 landcover (Fig. 8-C) and are similar to the spatial distribution of calculated indices (Fig. 3-D to 3-I). This indicates that the MCASD analysis provided a means to visualise all 13 bands of these complex data sources in a comparable way to recognised methods.

The cluster vector signatures for both S2 MCASD results were overlain on a single plot (Fig. 8-D). The absolute values for the cluster signatures were very similar. The main difference is the S2 rededge1 (B5) data band were significantly different between the two cluster signature results (Fig. 8-D).

The reason for the difference between the two data sources may be explained by differing environmental conditions. A heatwave was recorded in Ireland in 2018 (Met Eireann, 2018), resulting in an increase in drought conditions. The red edge part of the electromagnetic spectrum is sensitive to plant chlorophyll content and increased red edge reflectance can indicate vegetation stress (Filella and Penuelas, 1994). Here, this stress was highlighted in the increased B5 reflectance values noted in 2018 S2 results and generally lower values in B6-B8A, when compared to 2017 S2 results. This environmental difference might also explain the difference in appropriate cluster numbers (Fig. 5-A/B) between the two S2 data sources. The heatwave in 2018 may have caused less green vegetation (predominantly shrubs and birch trees (Bord na Móna, 2021)) in the area classified as "peat bogs" (Fig. 8-C), therefore changing the reflectance values and the MCASD results in this area.

Using two instances of S2 data sources served several purposes. Firstly, it allowed for a comparative analysis, alongside the correlation results (Table 2), to validate the use of S2 2017 data source when combined with a radiometric data source from the previous year. Secondly, it highlights the need for objective analysis when choosing the appropriate number of clusters for a data source. Thirdly, it highlighted the potential of the framework developed here to show temporal (gradual or sudden) (Watson et al., 2014) changes to peatland landcover, similar to that described in Bhatnagar et al. (2020), as the same analysis could be applied to seasonally averaged S2 data to show gradual

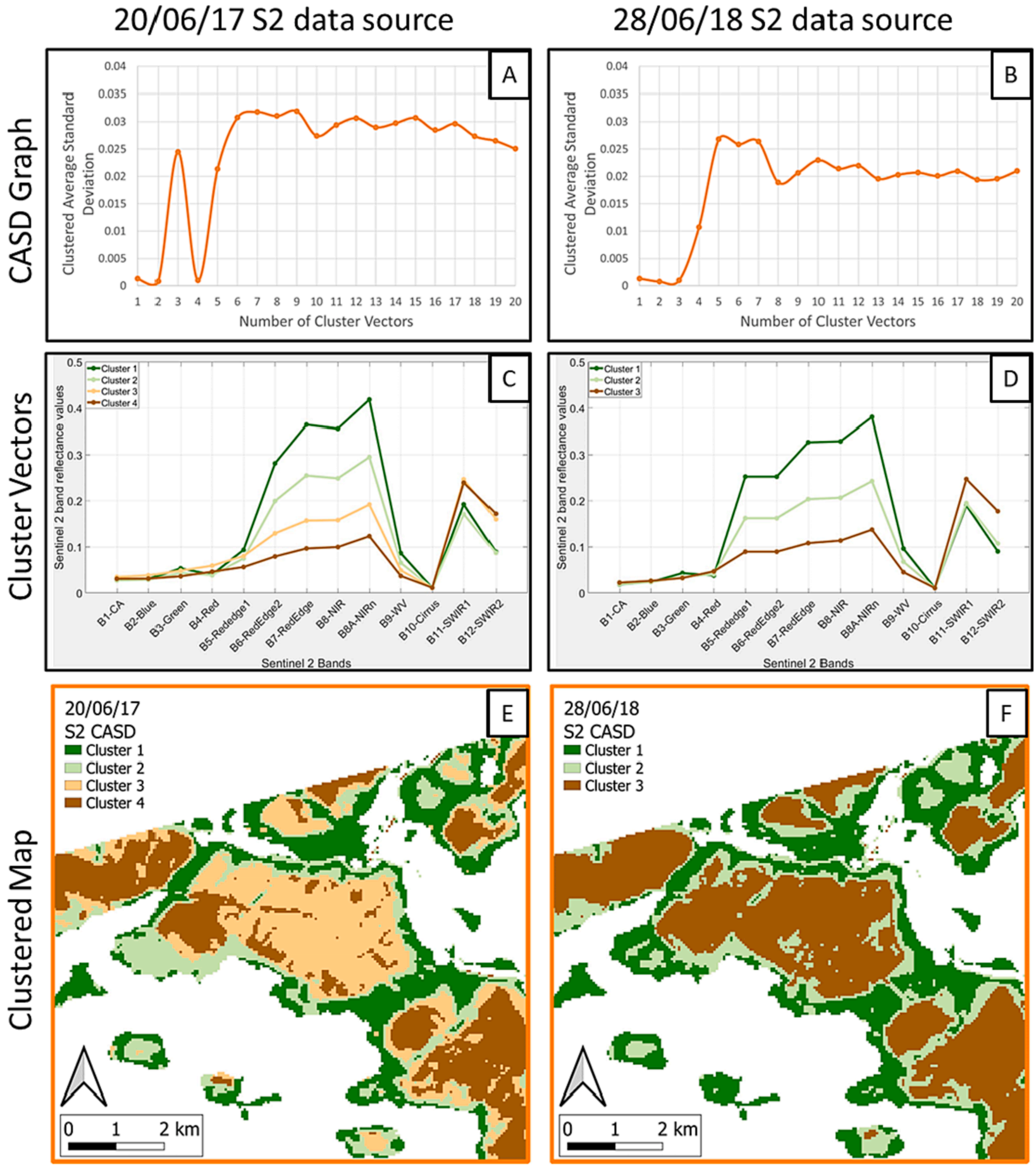

Fig. 5. MCASD analysis for two (2017 and 2018) S2 data sources. A-B) MCASD graph for maximum of 20 experimental cluster signatures. C-D) Cluster signatures for S2 bands. E-F) Spatial distribution of each clustering solution.

change, or to individual instances of S2 data to show sudden change.

4.2. Subsurface Intra-peatland variation of radiometric signal

Several studies have attempted to link the TC band in radiometric data to peat thickness. Gatis et al. (2019) combined this band with high resolution topography indices and Keaney et al. (2013) implemented a combined interpolation of this band with in-situ peat thickness measurements. Both studies reported mixed results and a decrease in confidence with increased peat thickness. Correlation analysis between radiometric data bands and peat thickness (section 3.1) indicated that the radiometric data bands were not sensitive to peat thickness variation

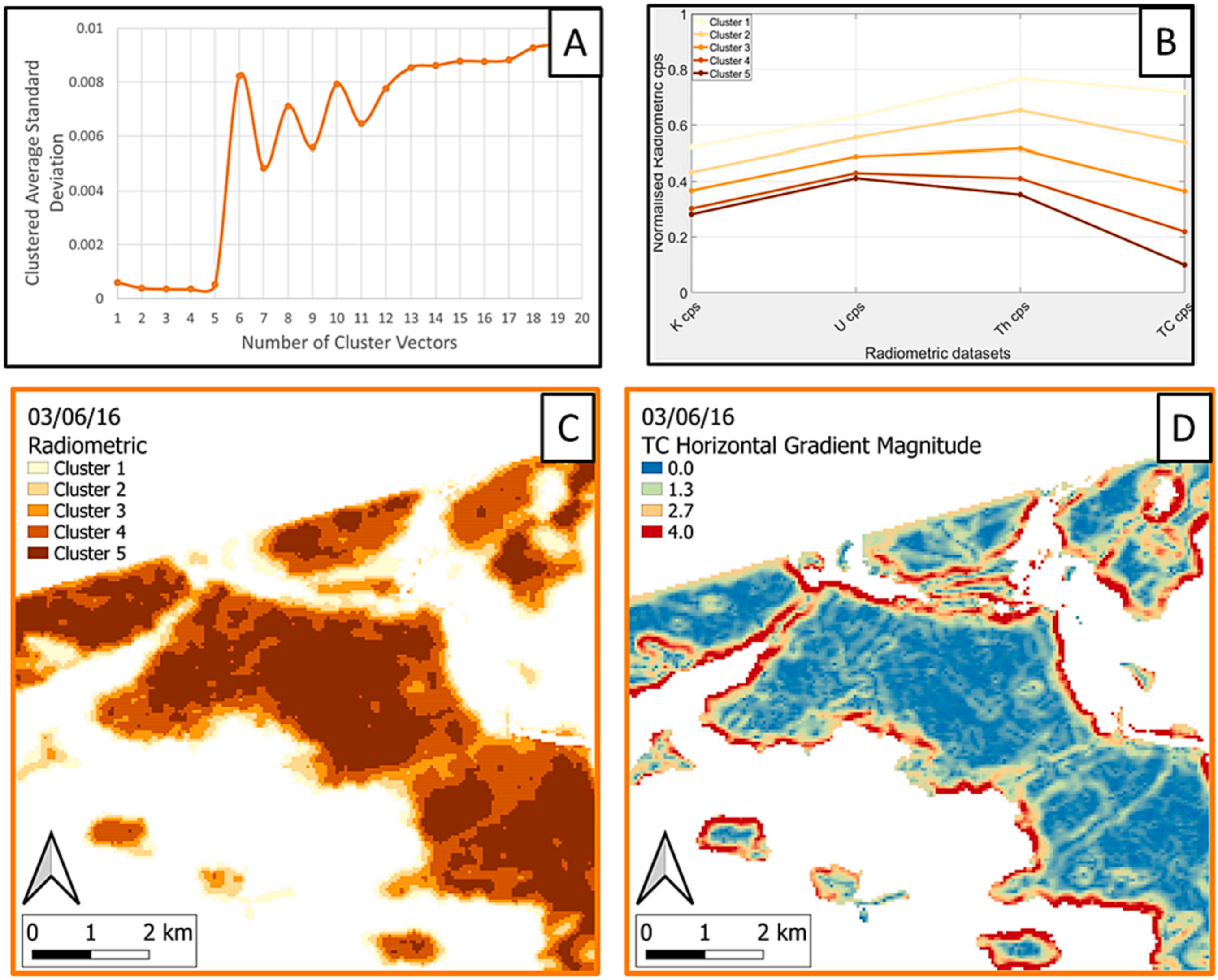

Fig. 6. MCASD analysis for radiometric data source. A) MCASD graph for maximum of 20 experimental cluster signatures. B) Normalised cluster signatures for radiometric data bands. C) Spatial distribution of the 5-cluster solution. D) Horizontal Gradient Magnitude Analysis of TC data band (Beamish, 2016) (Blue = low horizontal gradient, Red = High horizontal gradient).

at this site. This is likely due to peat thickness being consistently greater than ~ 60 cm (Bord na Móna, 2021).

Water has a ~ 10 % greater attenuation strength compared to geological material (Beamish, 2014; Endrestøl, 1980). Peat has very low bulk density (Kiely and Carton, 2010) and very high porosity (Galvin, 1976). The low bulk density further reduces the attenuation strength of the solid component of a peat soil (O'Leary et al., 2022), while high porosity provides pore space for high volumetric water content in the soil.

Vegetation may also have an attenuating effect on gamma rays (Minasny et al., 2019; Minty, 1997). This is an ongoing research area in the relatively new discipline of radiometric mapping of soils (Beamish, 2015; Rawlins et al., 2007). However, the effect was not noted in this study as clusters identified as having vegetation from CORINE 2018 landcover (Fig. 3-C) also had a high radiometric value, indicating less attenuation.

One means to analyse radiometric signal variation is the Horizontal Gradient Magnitude (Beamish, 2016) which highlights areas of changing radiometric signal (Fig. 6-D). This method, however, only uses a single data band (TC) and does not provide a means to spatially link areas of similar radiometric signal. In this study, the use of MCASD analysis included all radiometric data bands acquired over this site and determined they can be gathered into a maximum of five clusters (Fig. 6-A), highlighting the spatial distribution of these clusters in the landscape.

The spatial distribution of these clusters (Fig. 6-C) are qualitatively comparable to CORINE landcover (Fig. 3-C). Clusters 4 and 5 appear to follow the "peat bogs" classification. And Clusters 1, 2 and 3 appear to follow the vegetation classifications. However, the radiometric results are sensitive to subsurface physical properties. These results may indicate areas of similar soil moisture across the site, with Cluster 1 being least and Cluster 5 being most saturated. The use of airborne radiometric data was to provide a means to analyse the intra-peatland subsurface variation of soil moisture (Beamish, 2013; Endrestøl, 1980), a hydrological indicator in the context of peatland restoration monitoring.

4.3. *Integrated landcover and subsurface interpretation*

Traditional correlation is a linear link between data sources, however the complexity inherent in peatland (Price et al., 2003) results in the need for a non-linear algorithm, such as neural networks, to exploit any link. The combination of optical and radar satellite data has yielded increased confidence in water table depth prediction (Räsänen et al., 2022). However, satellite data sources only measure the very near

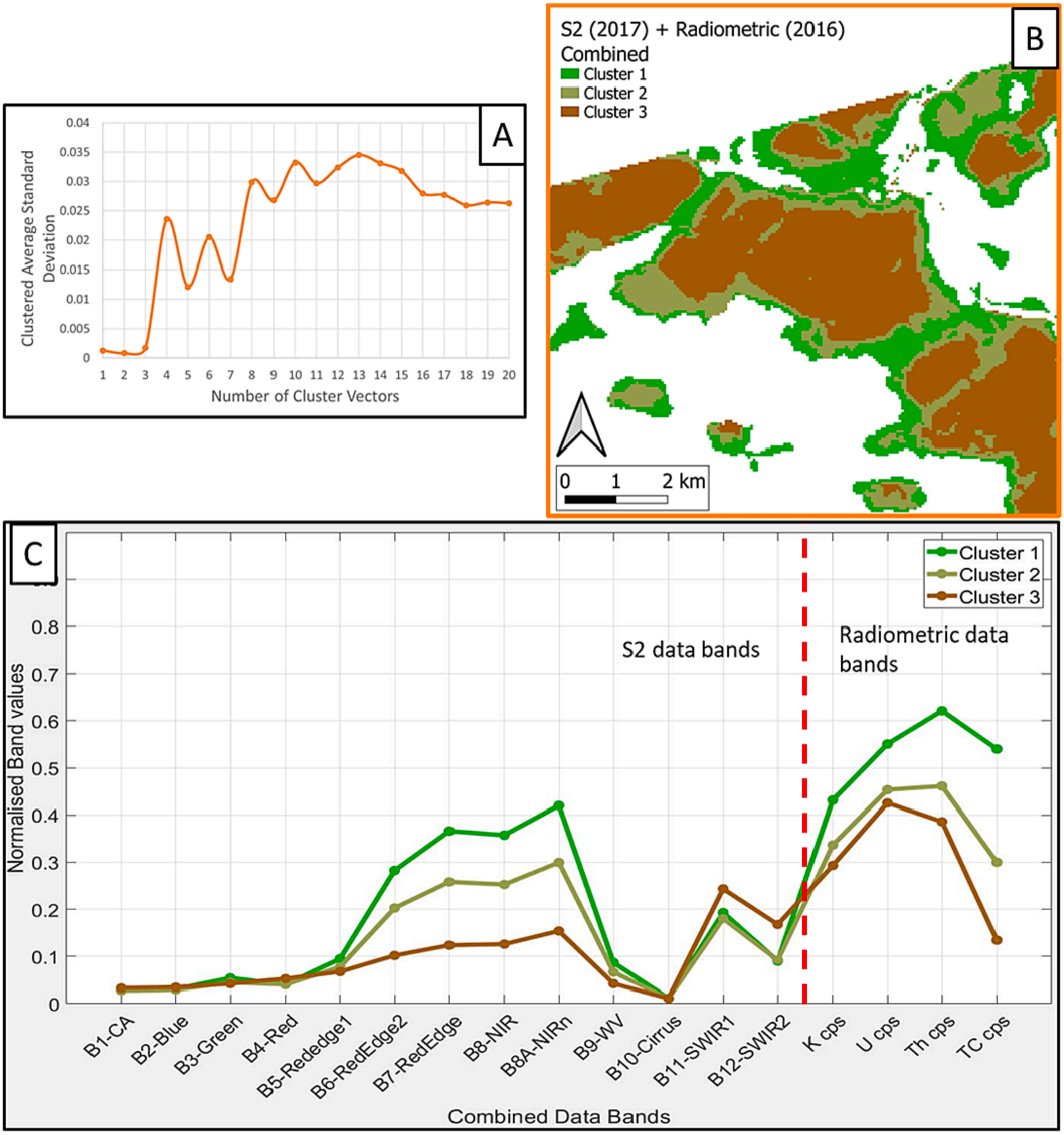

Fig. 7. MCASD analysis for combined S2 and radiometric data source. A) MCASD graph for maximum of 20 experimental cluster signatures. B) Spatial distribution of the 3-cluster solution C) Cluster signatures for all data bands (S2 bands are absolute values and radiometric bands are normalised values for ease of visualisation).

surface (Minasny et al., 2019) and must infer subsurface information. Radiometrics is a direct measurement of the subsurface and was combined with 2017 S2 in an unsupervised neural network.

The combined result (Fig. 7) represents an interpretation from land surface to subsurface depth of ~ 60 cm. The spatial distribution of the combined MCASD analysis closely followed the CORINE 2018 (Fig. 8-C) landcover, however there was increased resolution within the "peat bogs" landcover class. The cluster signature plot (Fig. 7-C) shows that the areas of strong vegetation response (B5 – B8A) in the S2 data bands are linked with the highest radiometric values, indicating less attenuation of radiometric signal in these areas. Areas of low vegetation response are linked to areas of strong radiometric attenuation, but the data do not rule out the possibility that near-surface (i.e., below ~ 2 mm) water might also be contributing to a low radiometric response.

S2 data also act as a proxy for soil moisture in the top few mm of the surface, specifically via the SWIR (B11 and B12) (Tian and Philpot, 2015), with increased soil moisture generally resulting in decreased reflectance in these bands. When compared to Clusters 1 & 2, a relative increase in B11 and 12 reflectance in Cluster 3 (Fig. 7-C), indicates a relative decrease in surface (~2 mm) moisture. However, this cluster also shows a relative decrease in radiometric response, indicating an increase in the subsurface (~60 cm) moisture. This validates a combined data source MCASD analysis to provide a full vegetation to surface to subsurface analysis and further highlights the advantage to including all 13 S2 data bands.

Based on the understanding of S2 and radiometric responses, the peatlands area is now classified into three clusters (Fig. 7). Cluster 1, which represents grass lands around the edge of the peatlands, likely with thin, dry peat and overlain by mineral soils. Cluster 2, which represents forested and/or grassland areas with wet soil, highlighted by a reduced radiometric response indicating either wetter or thicker peat material is present. And Cluster 3, which represents open peatlands

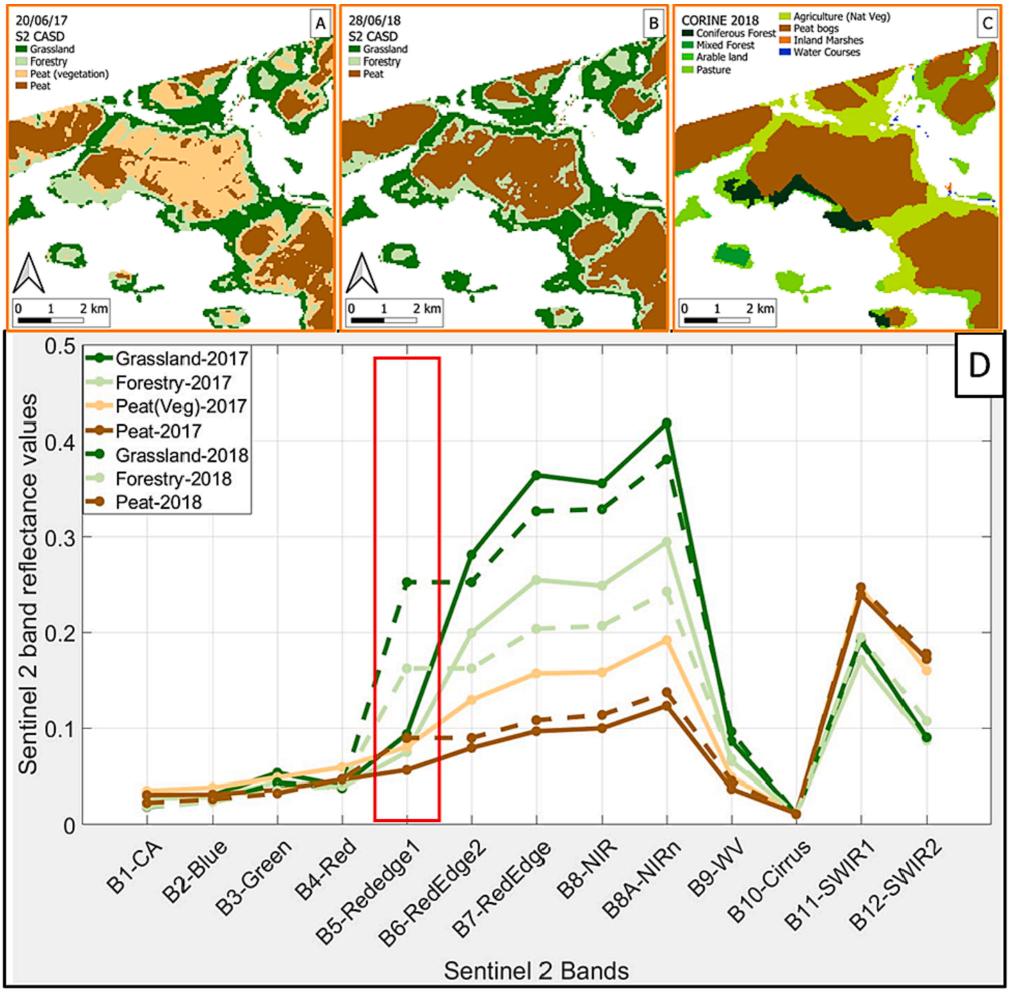

Fig. 8. A) Spatial distribution of 2017 S2 MCASD analysis. B) Spatial distribution of 2018 S2 MCASD analysis. C) CORINE 2018 landcover classification. D) Cluster vector signature plot (Solid lines = S2 2017 4 cluster result, Dashed lines = S2 2018 3 cluster result). Red box highlights B5-rededge. Grassland = CORINE 2018 "arable land", "Pasture", "Agriculture (Nat Veg)" classes. Forestry = CORINE 2018 "Coniferous Forest", "Mixed Forest" classes. Peat and Peat (Veg) = CORINE 2018 "Peat bogs" class.

areas, with limited vegetation, relatively low surface soil moisture, and relatively high subsurface soil moisture.

4.4. *Implications for and beyond peatland monitoring*

The combined MCASD analysis has provided a data driven, semi-automatic method to analyse multiple data sources. In the context of peatlands, once a peatland extent has been identified, this framework may provide a tool to monitor peatland restoration (Mackin et al., 2017) by providing a set of baseline conditions prior to restoration, as well as temporal monitoring during and after restoration (Bhatnagar et al., 2020). Other temporally and spatially coincident data sources may also be integrated to this framework.

Sentinel 1 radar backscatter data may provide soil moisture information to ~ 10 cm depth (Bauer-Marschallinger et al., 2019; Bechtold et al., 2018). However, currently the noise in this source of data results in a spatial resolution which is not ideal for plot scale studies. Airborne electromagnetic measurements may be able to estimate peat thickness (Boaga et al., 2020; Siemon et al., 2020), however often vertical resolution is an issue, especially in areas with thin peats.

This study highlights the difficulties of acquiring satellite-based optical data in temperate areas with persistent cloud cover (Connolly, 2019). One way around this would be to acquire coincident optical and radiometric data bands using airborne or drone platforms (Dronova et al., 2021; Mustaffa et al., 2020; von Hebel et al., 2021). This could provide a temporally and spatially coincident data source, which is repeatable throughout the lifecycle of a restoration project.

Restoration of peatlands aims to return these sites to near natural conditions including reintroduction of peatland habitats (Renou-Wilson et al., 2019) and maintaining a water table at ~ 10 cm depth (Evans et al., 2021). Repeat MCASD analysis of optical (landcover) and radiometric (soil moisture) measurements (as well as other relevant datasets), may provide a useful tool in monitoring vegetation and water table levels over time, both indicators of restoration success (Mackin et al., 2017).

The methods presented in this article have application beyond the scope of peatland restoration and may be useful in any environment that requires a multi-sensor approach to analysis such as soil mapping (Brogi et al., 2019) and precision agriculture (von Hebel et al., 2021).

5. Conclusions

This paper has developed a new metric, Multi-Cluster Average Standard Deviation (MCASD), to facilitate the choice of the most appropriate number of clusters in an unsupervised classification of data from multiple sources. It demonstrates how stable clusters with the highest spatial resolution can be generated with, for example, Self-Organising Maps. The method was demonstrated using different combinations of optical satellite and airborne radiometric data over a peatland but has implications for many research domains such as seabed mapping, precision agriculture and any discipline utilising multi-dimensional geospatial data.

The use of machine learning neural networks in this study allowed for an objective analysis of intra-peatland variability of all data bands from S2 optical data. Self-Organising Maps produces a "spectral signature" for each cluster highlighting differences in spectral bands. This "full spectrum" approach does not rely on only specific spectral bands of S2 data, as with indices such as NDVI, but can be used to show a comprehensive and visually simple view of the spatial and temporal variations in all S2 data bands across a site, highlighted here by B5 differences indicating vegetation stress due to a heatwave.

The same Self-Organising Maps approach was applied to intra-peatland variation of radiometric signal. This resulted in a multi-variate, quantitative means of linking areas of similar radiometric signal with the main advantage over traditional Horizontal Gradient Magnitude being the means to visualise variations in four bands of radiometric data simultaneously. Variation in radiometric signal on this site was most likely due to soil moisture.

The combination of these two data sources within the MCASD method produced a comprehensive, integrated interpretation of intra-peatland variation of ecological and hydrological factors without the need for an extensive ground data collection campaign. An S2 data source from 2017 provided a proxy for surface vegetation and soil moisture levels across the study site, while radiometric data acted as a proxy for subsurface soil moisture to ~ 60 cm. The combination of these two data sources within an MCASD analysis resulted in the division of this peatlands site into three distinct zones of differing surface and subsurface conditions (Fig. 7).

This study provides the framework for monitoring peatland habitat restoration, especially when considering spatially and temporally coincident, high resolution acquisition platforms, such as drones.

Declaration of Competing Interest

The authors declare that they have no known competing financial interests or personal relationships that could have appeared to influence the work reported in this paper.

Data availability

Data will be made available on request.

Acknowledgement

The research conducted in this publication was funded by the Irish Research Council under grant number GOIPG-2018-233. Contains Irish Public Sector Data (Geological Survey Ireland) licensed under a Creative Commons Attribution 4.0 International (CC BY 4.0) licence. Peat thickness data was provided to the authors by Bord na Móna.

Appendix A. Supplementary data

Supplementary data to this article can be found online at https://doi.org/10.1016/j.geoderma.2023.116348.

References

Airo, M.-L., Hyvönen, E., Lerssi, J., Leväniemi, H., Ruotsalainen, A., 2014. Tips and tools for the application of GTK's airborne geophysical data. accessed 09/05/2022 Geological Survey of Finland. https://tupa.gtk.fi/julkaisu/tutkimusraportti/tr_215.pdf,.

Altdorff, D., Bechtold, M., van der Kruk, J., Vereecken, H., Huisman, J.A., 2016. Mapping peat layer properties with multi-coil offset electromagnetic induction and laser scanning elevation data. Geoderma 261, 178–189. https://doi.org/10.1016/j.geoderma.2015.07.015.

Ameglio, L., 2018. Review of developments in airborne geophysics and geomatics to map variability of soil properties. 14th International Conference on Precision Agriculture, https://www.ispag.org/proceedings/?action=download&item=5024, (accessed 14/04/2022).

Arekhi, M., Goksel, C., Sanli, F.B., Senel, G., 2019. Comparative Evaluation of the Spectral and Spatial Consistency of Sentinel-2 and Landsat-8 OLI Data for Igneada Longos Forest. Isprs Int J Geo-Inf 8 (2). https://doi.org/10.3390/ijgi8020056.

Aune-Lundberg, L., Strand, G.H., 2021. The content and accuracy of the CORINE Land Cover dataset for Norway. International Journal of Applied Earth Observation and Geoinformation 96. https://doi.org/10.1016/j.jag.2020.102266.

Bauer-Marschallinger, B., Freeman, V., Cao, S., Paulik, C., Schaufler, S., Stachl, T., Modanesi, S., Massario, C., Ciabatta, L., Brocca, L., Wagner, W., 2019. Toward Global Soil Moisture Monitoring With Sentinel-1: Harnessing Assets and Overcoming Obstacles. Ieee T Geosci Remote 57 (1), 520–539. https://doi.org/10.1109/TGRS.2018.2858004.

Beamish, D., 2013. Gamma ray attenuation in the soils of Northern Ireland, with special reference to peat. J Environ Radioactiv 115, 13–27. https://doi.org/10.1016/j.jenvrad.2012.05.031.

Beamish, D., 2014. Peat Mapping Associations of Airborne Radiometric Survey Data. Remote Sens-Basel 6 (1), 521–539. https://doi.org/10.3390/rs6010521.

Beamish, D., 2016. Enhancing the resolution of airborne gamma-ray data using horizontal gradients. Journal of Applied Geophysics 132, 75–86. https://doi.org/10.1016/j.jappgeo.2016.07.006.

Beamish, D., Young, M., 2009. Geophysics of Northern Ireland - the Tellus Effect. First Break 27 (8). https://doi.org/10.3997/1365-2397.27.1302.32176.

Beamish, D., 2015. Relationships between gamma-ray attenuation and soils in SW England. Geoderma 259, 174-186. https://doi.org/10.1016%2Fj.geoderma.2015.05.018.

Bechtold, M., Schlaffer, S., Tiemeyer, B., De Lannoy, G., 2018. Inferring Water Table Depth Dynamics from ENVISAT-ASAR C-Band Backscatter over a Range of Peatlands from Deeply-Drained to Natural Conditions. Remote Sens-Basel 10 (4). https://doi.org/10.3390/rs10040536.

Benabdellah, A.C., Benghabrit, A., Bouhaddou, I., 2019. A survey of clustering algorithms for an industrial context. Procedia Computer Science 148, 291–302. https://doi.org/10.1016/j.procs.2019.01.022.

Berglund, O., Berglund, K., 2010. Distribution and cultivation intensity of agricultural peat and gyttja soils in Sweden and estimation of greenhouse gas emissions from cultivated peat soils. Geoderma 154 (3–4), 173–180. https://doi.org/10.1016/j.geoderma.2008.11.035.

Bhatnagar, S., Gill, L., Regan, S., Naughton, O., Johnston, P., Waldren, S., Ghosh, B., 2020. Mapping vegetation communities inside Wetlands using Sentinel-2 imagery in Ireland. International Journal of Applied Earth Observation and Geoinformation 88, 102083. https://doi.org/10.1016/j.jag.2020.102083.

Binley, A., Hubbard, S., Huisman, J., Revil, A., Robinson, D., Singha, K., Slater, L., 2015. The emergence of hydrogeophysics for improved understanding of subsurface processes over multiple scales. Water Resources Research 51 (6), 3837–3866. https://doi.org/10.1002/2015WR017016.

Boaga, J., Viezzoli, A., Cassiani, G., Deidda, G.P., Tosi, L., Silvestri, S., 2020. Resolving the thickness of peat deposits with contact-less electromagnetic methods: A case study in the Venice coastland. Science of the Total Environment 737. https://doi.org/10.1016/j.scitotenv.2020.139361.

Bord na Móna, 2021. Garryduff Decommissioning and Rehabilitation Plan 2021, https://www.bnmpcas.ie/wp-content/uploads/sites/18/2021/08/Garryduff-Rehab-Plan-V8.pdf, (accessed 17/05/2022).

Brogi, C., Huisman, J.A., Patzold, S., von Hebel, C., Weihermuller, L., Kaufmann, M.S., van der Kruk, J., Vereecken, H., 2019. Large-scale soil mapping using multi-configuration EMI and supervised image classification. Geoderma 335, 133–148. https://doi.org/10.1016/j.geoderma.2018.08.001.

Caliński, T., Harabasz, J., 1974. A dendrite method for cluster analysis. Communications in Statistics 3 (1), 1–27. https://doi.org/10.1080/03610927408827101.

Chatfield, C., 1986. Exploratory data analysis. European Journal of Operational Research 23 (1), 5–13. https://doi.org/10.1016/0377-2217(86)90209-2.

Chavez, P.S., 1996. Image-Based Atmospheric Corrections - Revisited and Improved. Photogrammetric Engineering and Remote Sensing 62, 1025–1036. https://doi.org/10.4236/acs.2016.62026.

Congedo, L., 2021. Semi-Automatic Classification Plugin: A Python tool for the download and processing of remote sensing images in QGIS. Journal of Open Source Software 6 (64), 3172. https://doi.org/10.21105/joss.03172.

Connolly, J., 2019. Mapping land use on Irish peatlands using medium resolution satellite imagery. Irish Geography; Vol 51, No 2 (2018): Special Issue - The vulnerability of Irish landscape systems to climate change and human activity - Part 1DO - 10.2014/igj.v51i2.1371, http://www.irishgeography.ie/index.php/irishgeography/article/view/1371, (accessed.

Corine, 2018. European Union, Copernicus Land Monitoring Service 2018. accessed 02/03/2022. https://land.copernicus.eu/.

Czapiewski, S., Szumińska, D., 2022. An Overview of Remote Sensing Data Applications in Peatland Research Based on Works from the Period 2010–2021. Land 11 (1). https://doi.org/10.3390/land11010024.

Davies, D.L., Bouldin, D.W., 1979. A Cluster Separation Measure. IEEE Transactions on Pattern Analysis and Machine Intelligence PAMI-1(2), 224–227. https://doi.org/10.1109/TPAMI.1979.4766909.

Delgado, S., Higuera, C., Calle-Espinosa, J., Morán, F., Montero, F., 2017. A SOM prototype-based cluster analysis methodology. Expert Systems With Applications 88, 14–28. https://doi.org/10.1016/j.eswa.2017.06.022.

Dramsch, J.S., 2020. 70 years of machine learning in geoscience in review. Advances in Geophysics 61. https://doi.org/10.1016/bs.agph.2020.08.002.

Dronova, I., Kislik, C., Dinh, Z., Kelly, M., 2021. A Review of Unoccupied Aerial Vehicle Use in Wetland Applications: Emerging Opportunities in Approach, Technology, and Data. Drones 5 (2). https://doi.org/10.3390/drones5020045.

Endrestøl, G.O., 1980. Principle and method for measurement of snow water equivalent by detection of natural gamma radiation / Principe et méthode pour la mesure de l'hauteur d'eau équivalente par détection du rayonnement gamma naturel. Hydrological Sciences Bulletin 25 (1), 77–83. https://doi.org/10.1080/02626668009491906.

Evans, C.D., Peacock, M., Baird, A.J., Artz, R.R.E., Burden, A., Callaghan, N., Chapman, P.J., Cooper, H.M., Coyle, M., Craig, E., Cumming, A., Dixon, S., Gauci, V., Grayson, R.P., Helfter, C., Heppell, C.M., Holden, J., Jones, D.L., Kaduk, J., Levy, P., Matthews, R., McNamara, N.P., Misselbrook, T., Oakley, S., Page, S.E., Rayment, M., Ridley, L.M., Stanley, K.M., Williamson, J.L., Worrall, F., Morrison, R., 2021. Overriding water table control on managed peatland greenhouse gas emissions. Nature 593 (7860), 548–552. https://doi.org/10.1038/s41586-021-03523-1.

Filella, I., Penuelas, J., 1994. The red edge position and shape as indicators of plant chlorophyll content, biomass and hydric status. International Journal of Remote Sensing 15 (7), 1459–1470. https://doi.org/10.1080/01431169408954177.

Frampton, W.J., Dash, J., Watmough, G., Milton, E.J., 2013. Evaluating the capabilities of Sentinel-2 for quantitative estimation of biophysical variables in vegetation. ISPRS Journal of Photogrammetry and Remote Sensing 82, 83–92. https://doi.org/10.1016/j.isprsjprs.2013.04.007.

Galvin, L.F., 1976. Physical-Properties of Irish Peats. Irish J Agr Res 15(2), 207-&, http://www.jstor.org/stable/25555820 . (accessed 09/05/2022).

Gao, X., Huete, A.R., Ni, W., Miura, T., 2000. Optical-Biophysical Relationships of Vegetation Spectra without Background Contamination. Remote Sens Environ 74 (3), 609–620. https://doi.org/10.1016/S0034-4257(00)00150-4.

Gatis, N., Luscombe, D.J., Carless, D., Parry, L.E., Fyfe, R.M., Harrod, T.R., Brazier, R.E., Anderson, K., 2019. Mapping upland peat depth using airborne radiometric and lidar survey data. Geoderma 335, 78–87. https://doi.org/10.1016/j.geoderma.2018.07.041.

Gersho, A., 1982. On the structure of vector quantizers. IEEE Transactions on Information Theory 28 (2), 157–166. https://doi.org/10.1109/TIT.1982.1056457.

Gsi, 2022a. National Bedrock Map 1:100K. accessed 01/05/2022. https://www.gsi.ie/en-ie/data-and-maps/Pages/Bedrock.aspx#100k.

Gsi, 2022b. National Quaternary Sedement Map 1:50K. accessed 02/05/2022. https://www.gsi.ie/en-ie/data-and-maps/Pages/Quaternary.aspx#Sed.

Gsi, 2022c. Tellus Survey. accessed 01/05/2022. https://www.gsi.ie/en-ie/programmes-and-projects/tellus/Pages/default.aspx.

Heger, T., Jeschke, J.M., Febria, C., Kollmann, J., Murphy, S., Rochefort, L., Shackelford, N., Temperton, V.M., Higgs, E., 2022. Mapping and assessing the knowledge base of ecological restoration. Restoration Ecology n/a(n/a) e13676.

Hird, J.N., DeLancey, E.R., McDermid, G.J., Kariyeva, J., 2017. Google Earth Engine, Open-Access Satellite Data, and Machine Learning in Support of Large-Area Probabilistic Wetland Mapping. Remote Sens-Basel 9(12). https://doi.org/10.3390/rs9121315.

Huete, A.R., 2004. Remote Sensing for Environmental Monitoring. In: Artiola, J.F., Pepper, I.L., Brusseau, M.L. (Eds.), Environmental Monitoring and Characterization. Academic Press, Burlington, pp. 183–206. https://doi.org/10.1016/B978-012064477-3/50013-8.

Iaea, 2003. Guidelines for Radioelement Mapping Using Gamma Ray Spectrometry Data. INTERNATIONAL ATOMIC ENERGY AGENCY, Vienna https://www.iaea.org/publications/6746/guidelines-for-radioelement-mapping-using-gamma-ray-spectrometry-data, (accessed 16/04/2022.

Kasischke, E.S., Bourgeau-Chavez, L.L., Rober, A.R., Wyatt, K.H., Waddington, J.M., Turetsky, M.R., 2009. Effects of soil moisture and water depth on ERS SAR backscatter measurements from an Alaskan wetland complex. Remote Sens Environ 113 (9), 1868–1873. https://doi.org/10.1016/j.rse.2009.04.006.

Kaufman, L., 2005. Finding groups in data an introduction to cluster analysis. Hoboken, N.J. : Wiley-Interscience, Hoboken, N.J. https://doi.org/10.1002/9780470316801.

Keaney, A., McKinley, J., Graham, C., Robinson, M., Ruffell, A., 2013. Spatial statistics to estimate peat thickness using airborne radiometric data. Spat Stat-Neth 5, 3–24. https://doi.org/10.1016/j.spasta.2013.05.003.

Kiang, M.Y., 2001. Extending the Kohonen self-organizing map networks for clustering analysis. Comput Stat Data An 38 (2), 161–180. https://doi.org/10.1016/S0167-9473(01)00040-8.

Kiely, G., Carton, O., 2010. SoilC - Measurement and Modelling of Soil Carbon Stocks and Stock Changes in Irish Soils, https://www.epa.ie/publications/research/land-use-soils-and-transport/soilc—measurement-and-modelling-of-soil-carbon-stocks-and-stock-changes-in-irish-soils.php, (accessed 09/05/2022).

Kohonen, T., 2013. Essentials of the self-organizing map. Neural Networks 37, 52–65. https://doi.org/10.1016/j.neunet.2012.09.018.

Kreyling, J., Tanneberger, F., Jansen, F., van der Linden, S., Aggenbach, C., Bluml, V., Couwenberg, J., Emsens, W.J., Joosten, H., Klimkowska, A., Kotowski, W., Kozub, L., Lennartz, B., Liczner, Y., Liu, H., Michaelis, D., Oehmke, C., Parakenings, K., Pleyl, E., Poyda, A., Raabe, S., Rohl, M., Rucker, K., Schneider, A., Schrautzer, J., Schroder, C., Schug, F., Seeber, E., Thiel, F., Thiele, S., Tiemeyer, B., Timmermann, T., Urich, T., van Diggelen, R., Vegelin, K., Verbruggen, E., Wilmking, M., Wrage-Monnig, N., Wolejko, L., Zak, D., Jurasinski, G., 2021. Rewetting does not return drained fen peatlands to their old selves. Nat Commun 12 (1). https://doi.org/10.1038/s41467-021-25619-y.

Liu, H.Q., Huete, A., 1995. A feedback based modification of the NDVI to minimize canopy background and atmospheric noise. Ieee T Geosci Remote 33 (2), 457–465. https://doi.org/10.1109/TGRS.1995.8746027.

Mackin, F., Barr, A., Rath, P., Eakin, M., Ryan, J., Jeffrey, R. & Fernandez Valverde, F., 2017. Irish Wildlife Manual No. 99: Best practice in raised bog restoration in Ireland, https://www.npws.ie/sites/default/files/publications/pdf/IWM99_RB_Restoration_Best%20Practice%20Guidance.pdf, (accessed 20/08/2022).

Maduako, I.N., Ndukwu, R.I., Ifeanyichukwu, C., Igbokwe, O., 2017. Multi-Index Soil Moisture Estimation from Satellite Earth Observations: Comparative Evaluation of the Topographic Wetness Index (TWI), the Temperature Vegetation Dryness Index (TVDI) and the Improved TVDI (iTVDI). J Indian Soc Remote 45 (4), 631–642. https://doi.org/10.1007/s12524-016-0635-9.

Marchant, B.P., 2021. Using remote sensors to predict soil properties: Radiometry and peat depth in Dartmoor. UK. Geoderma 403, 115232. https://doi.org/10.1016/j.geoderma.2021.115232.

Marsh, I., Brown, C., 2009. Neural network classification of multibeam backscatter and bathymetry data from Stanton Bank (Area IV). Appl Acoust 70 (10), 1269–1276. https://doi.org/10.1016/j.apacoust.2008.07.012.

Martelet, G., Truffert, C., Tourliere, B., Ledru, P., Perrin, J., 2006. Classifying airborne radiometry data with Agglomerative Hierarchical Clustering: A tool for geological mapping in context of rainforest (French Guiana). International Journal of Applied Earth Observation and Geoinformation 8 (3), 208–223. https://doi.org/10.1016/j.jag.2005.09.003.

Met Eireann, 2018. Summer 2018 Analysis (accessed 19/09/2022). https://www.met.ie/summer-2018-analysis.

Minasny, B., Berglund, O., Connolly, J., Hedley, C., de Vries, F., Gimona, A., Kempen, B., Kidd, D., Lilja, H., Malone, B., McBratney, A., Roudier, P., O'Rourke, S., Rudiyanto, Padarian, J., Poggio, L., ten Caten, A., Thompson, D., Tuve, C., Widyatmanti, W., 2019. Digital mapping of peatlands - A critical review. Earth-Sci Rev 196. https://doi.org/10.1016/j.earscirev.2019.05.014.

Minty, B.R.S., 1997. Fundamentals of airborne gamma-ray spectrometry. accessed 09/05/2022 AGSO Journal of Australian Geology and Geophysics 17 (2), 39–50. http://inis.iaea.org/search/search.aspx?orig_q=RN:28049082,.

Monteverde, S., Healy, M.G., O'Leary, D., Daly, E., Callery, O., 2022. Management and rehabilitation of peatlands: The role of water chemistry, hydrology, policy, and emerging monitoring methods to ensure informed decision making. Ecological Informatics 69, 101638. https://doi.org/10.1016/j.ecoinf.2022.101638.

Mustaffa, A.A., Mukhtar, A.N., Rasib, A.W., Suhandri, H.F., Bukari, S.M., 2020. Mapping of Peat Soil Physical Properties by Using Drone- Based Multispectral Vegetation Imagery. IOP Conference Series: Earth and Environmental Science 498 (1), 012021. https://doi.org/10.1088/1755-1315/498/1/012021.

O'Leary, D., Brown, C., Daly, E., 2022. Digital soil mapping of peatland using airborne radiometric data and supervised machine learning – implication for the assessment of carbon stock. Geoderma 428. https://doi.org/10.1016/j.geoderma.2022.116086.

Price, J., Heathwaite, A., Baird, A., 2003. Hydrological processes in abandoned and restored peatlands: an overview of management approaches. Wetlands Ecology and Management 11 (1–2), 65–83. https://doi.org/10.1023/A:1022046409485.

Priori, S., Bianconi, N., Costantini, E.A.C., 2014. Can γ-radiometrics predict soil textural data and stoniness in different parent materials? A comparison of two machine-learning methods. Geoderma 226–227, 354–364. https://doi.org/10.1016/j.geoderma.2014.03.012.

Qiu, C.J., Zhu, D., Ciais, P., Guenet, B., Peng, S.S., 2020. The role of northern peatlands in the global carbon cycle for the 21st century. Global Ecol Biogeogr 29 (5), 956–973. https://doi.org/10.1111/geb.13081.

Räsänen, A., Tolvanen, A., Kareksela, S., 2022. Monitoring peatland water table depth with optical and radar satellite imagery. International Journal of Applied Earth Observation and Geoinformation 112, 102866. https://doi.org/10.1016/j.jag.2022.102866.

Rawlins, B.G., Lark, R.M., Webster, R., 2007. Understanding airborne radiometric survey signals across part of eastern England. Earth Surf Proc Land 32 (10), 1503–1515. https://doi.org/10.1002/esp.1468.

Reinhardt, N., Herrmann, L., 2019. Gamma-ray spectrometry as versatile tool in soil science: A critical review. J Plant Nutr Soil Sc 182 (1), 9–27. https://doi.org/10.1002/jpln.201700447.

Renou-Wilson, F., Moser, G., Fallon, D., Farrell, C.A., Müller, C., Wilson, D., 2019. Rewetting degraded peatlands for climate and biodiversity benefits: Results from two raised bogs. Ecological Engineering 127, 547–560. https://doi.org/10.1016/j.ecoleng.2018.02.014.

Sentinel, 2022. Sentinel Overview. https://sentinel.esa.int/web/sentinel/missions, (accessed 18/08/2022).

SGL, 2017. Fixed-Wing High-Resolution Aeromagnetic, Gamma-ray Spectrometric and Frequency-Domain Electromagnetic Survey. In: G.S.o. Ireland (Ed.), https://secure.dccae.gov.ie/GSI_DOWNLOAD/Tellus/SGL_Tech_Report_831A2_000.pdf, (accessed 09/05/2022).

Shives, R.B.K., Charbonneau, B.W., Ford, K.L., 2000. The detection of potassic alteration by gamma-ray spectrometry - Recognition of alteration related to mineralization. Geophysics 65 (6), 2001–2011. https://doi.org/10.1190/1.1444884.

Siemon, B., Ibs-von Seht, M., Frank, S., 2020. Airborne Electromagnetic and Radiometric Peat Thickness Mapping of a Bog in Northwest Germany (Ahlen-Falkenberger Moor). Remote Sens-Basel 12 (2). https://doi.org/10.3390/rs12020203.

Tian, J., Philpot, W.D., 2015. Relationship between surface soil water content, evaporation rate, and water absorption band depths in SWIR reflectance spectra. Remote Sens Environ 169, 280–289. https://doi.org/10.1016/j.rse.2015.08.007.

Unep, 2022. Global Peatlands Assessment – The State of the World's Peatlands: Evidence for action toward the conservation, restoration, and sustainable management of peatlands. Main Report, United Nations Environment Programme, Nairobi https://wedocs.unep.org/bitstream/handle/20.500.11822/41222/peatland_assessment.pdf?sequence=1&isAllowed=y, (accessed 05/01/2023.

Unfccc, 2011. Consideration of further commitments for Annex I Parties under the Kyoto Protocol. accessed 16/08/2022. https://unfccc.int/documents/7085.

Valentine, A., Kalnins, L., 2016. An introduction to learning algorithms and potential applications in geomorphometry and Earth surface dynamics. Earth Surf Dynam 4 (2), 445–460. https://doi.org/10.5194/esurf-4-445-2016.

von Hebel, C., Reynaert, S., Pauly, K., Janssens, P., Piccard, I., Vanderborght, J., van der Kruk, J., Vereecken, H., Garre, S., 2021. Toward high-resolution agronomic soil information and management zones delineated by ground-based electromagnetic induction and aerial drone data. Vadose Zone J 20 (4). <Go to ISI>://WOS:000674053400011, (accessed.

Wang, L., Qu, J.J., 2009. Satellite remote sensing applications for surface soil moisture monitoring: A review. Frontiers of Earth Science in China 3 (2), 237–247. https://doi.org/10.1007/s11707-009-0023-7.

Watson, S.J., Luck, G.W., Spooner, P.G., Watson, D.M., 2014. Land-use change: incorporating the frequency, sequence, time span, and magnitude of changes into ecological research. Frontiers in Ecology and the Environment 12 (4), 241–249. https://doi.org/10.1890/130097.

Wilson, D., Mackin, F., Tuovinen, J.-P., Moser, G., Farrell, C., Renou-Wilson, F., 2022. Carbon and climate implications of rewetting a raised bog in Ireland. Global Change Biology n/a(n/a). https://doi.org/10.1111/gcb.16359.

Xing, G., Wang, X., Zhang, Y., Lu, C., Pless, R., Gill, C., 2005. Integrated coverage and connectivity configuration for energy conservation in sensor networks. ACM Trans. Sen. Netw. 1 (1), 36–72. https://doi.org/10.1145/1077391.1077394.

Xu, J.R., Morris, P.J., Liu, J.G., Holden, J., 2018. PEATMAP: Refining estimates of global peatland distribution based on a meta-analysis. Catena 160, 134–140. https://doi.org/10.1016/j.catena.2017.09.010.